FUSION OF TWO ILLUMINATION TECHNIQUES AND COMBINATION WITH ONE DATA PROCESSING TECHNIQUE FOR SMALL BOREHOLE INSPECTION

YANNICK CAULIER, ANDREAS PÖSCH, MARC ARNOLD, KLAUS SPINNLER

Abstract. Within the field of surface quality control, the automatic inspection of inner surfaces is a challenging task, as the necessary recording components have to be positioned in a small cavity in order to gain adequate images of the inner surfaces to be inspected. This increases the difficulty to define and realize the optimal, in terms of image quality and inspection speed, recording set-up. Furthermore, the simultaneous visual enhancement and discrimination of different defect types necessitates the use of at least two different lighting technologies.

This paper proposes a new methodology for visually enhancing and discriminating different defect types, situated in small cavities, in one shot. The proposed approach is based on the fusion of an existing system for inner surface inspection and a quality control method using structured light.

The proposed optimization process is dedicated to the retrieval of the optimal structured lighting in terms of 3D light shape, and geometry of the projected light structure. The achieved simulated results based on a ray-tracing approach, correlate with the laboratory recordings of a defective inner surface. Finally, the results demonstrate that the proposed methodology, based on the projection of an adapted structured lighting, permits the enhancement and discrimination of different inner surface defects.

1. Introduction

Inspecting small inner surfaces, i.e. of a few millimeter diameters, is a challenging task, as the necessary recording components (optics, lightings) have to be positioned in a small cavity in order to gain adequate images for the quality control of the inner surfaces to be inspected. Furthermore, inspection difficulty increases, if in addition to the visual enhancement task of defective surface parts, different types of defects have to be detected. Hence, appropriate hardware components, such as endoscopes or borescopes for inner surface recordings, combined with adequate image processing methods, as adapted lighting for surface discrimination, have to be developed.

Many applications in the domain of industrial as well as medical image processing make considerable use of rigid or flexible endoscopes - so called "borescopes" or "fiberscopes", see Fig. 1, - to gain visual access to holes, hollows, antrums and cavities that are difficult to enter and examine. Common to both application fields are usually very small man-made or natural entry points to the observed scene - with diameters below 4 mm - as well as the complexity of the hollow itself, necessitating the use of an adapted illumination. Due to the complex and bended shape of such

Key words and phrases. Inner Surfaces, Endoscopy, Borescope, Structured Illumination, Quality Control, Deflectometry.

FIGURE 1. Standard endoscopes (also called borescopes) with different diameters and typical industrial inner surface examples.

intrinsic cavities, only adapted solutions can be used for the examination of these hollows. In the industrial machine inspection, typical examples are complex drill holes and coolant bores in turbine blades [6, 4, 1, 8].

Within the context of industrial surface inspection, a human inspector typically places the object to be inspected under appropriate lighting to visually enhance the defective parts, in order to identify different surface defects, e.g. textural or geometrical ones. Most machine vision solutions are based on the same principle, which consists of using the deflection of the light rays in order to distinguish the acceptable and non-acceptable surfaces. Examples of such an inspection principle, used for industrial inline inspection can be found in [10, 3]. Typical applications are as e.g. the inspection of metallic car parts [7], large steel plates [5] or steel cylinder surfaces [2].

However, none of the cited applications, address the real-time inline inspection (complex calibration procedure) for the simultaneous detection of different defect types (non-adapted lighting) situated on inner, i.e. badly accessible, surfaces.

Concerning the inline inspection of inner surfaces, but also the development and integration of combined lighting and data processing methods, two major and reference systems were developed. The former [9] permits the inspection of small inner surfaces, with a diameter of up to approximately 2 mm, whereas the latter [11, 12] uses the projection onto the surface to be inspected, of a stripe illumination pattern, fusion of a diffuse and a structured light, for its direct characterization in terms of defective surfaces visual enhancement. It has been demonstrated that the former method outperforms other similar approaches dedicated to the inline inspection of inner surfaces, and that the principle of the latter can be generalized to further inspection tasks. The major points of this paper are:

- to demonstrate that both quality control approaches can be fused,
- to propose a miniaturized and multimodal lighting for inner surface quality control,

- and to demonstrate that this approach can be used for inline real-time inspection.

This paper is organized into 4 sections. Section 2 describes the problem to be solved, section 3 addresses the retrieval of the most optimal light structure, section 4 shows the simulated results and the achieved laboratory recording. Section 5 summarizes and concludes this paper.

2. Description of the method

2.1. **Principle of the endoscopy recording.** The endoscopic inspection permits the control or examination of small cavities or boreholes by means of an endoscope, which is a thin, long (sometimes flexible) tube. The endoscope is linked with a light source and a camera, in order to relayed the badly accessible illuminated inner surfaces to an external PC.

In case of industrial recordings for continuous surface inspection, the common approach consists of fixing the object to be inspected, and moving the camera and the lighting with a constant speed and distance through the surface. Indeed, in most cases the complete inner wall of the tube, cannot be recorded by a single shot, as tube length is often much higher than the distance between the distal end of the borescope and the light source. Afterwards, all the recorded images have to be dewarped, to remove the optical distortions, and stitched together, in order to get a view of the complete inner surface.

Fig. 2 shows the endoscopic recording principle and the deflectometry-based quality control. The figure depicts the recording principle of an inner surface. Camera and light source are moving simultaneously, i.e. with constant speed and mutual distance, along the tube's axis. The deflectometric quality control principle is explained in the next section.

2.2. **Principle of deflectometry for quality control.** The illumination, result of the fusion of a diffuse and structured light, for the simultaneous visual enhancement of different defect types is described in [12]. The cases of geometrical 3D and textural 2D defects which were considered, are depicted in Fig. 2. For all the rest of the paper, these two defect types will be used. The generalization to further defect types is straightforward.

The surface visual enhancement principle, is based on the deviation and the absorption of the projected light rays onto the surface to be inspected. Hence, such an object inspection using a specular lighting technique, is applied for reflective surfaces with a non-negligible value of reflectance coefficient ρ. ρ expresses the percentage of the reflected to the projected flux of light. This coefficient is null for diffuse surfaces which reflect the light in any direction i.e. as Lambertian sources. For a specular reflection the angle of the reflected component is equal to the angle of the incident beam with respect to the surface normal $\overrightarrow{\mathbf{N}}$.

The disturbances of the projected light pattern are therefore directly linked with the illuminated object surface types. We call (s) an elementary surface element of object surface S to be inspected. ρ_s and α_s are the reflectance coefficient and the reflection angle of surface element s. Fig. 2 uses 3 examples illustrating ideal reflection conditions of a reflected ray on a surface element s.

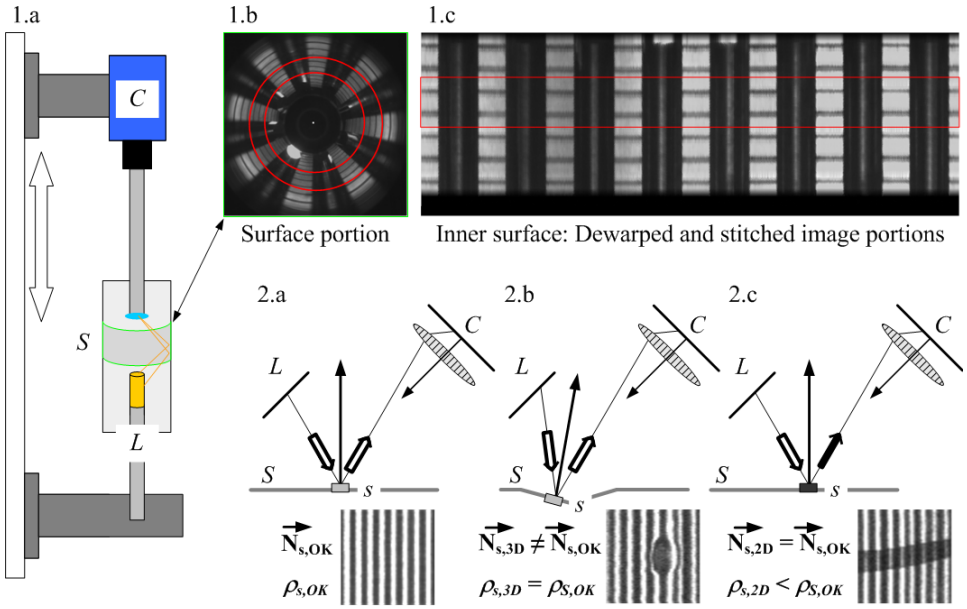

FIGURE 2. Images 1: Principle of inner surface endoscopic recording. Camera C and light L move with a constant speed in order to record the inner object surface. Only a portion of an image, containing the relevant information, is dewarped and stitched. Images 2: Deflectometry principle for quality control. The surface interpretation features, are the deviations and the intensity of the projected light structure. Both are linked to geometrical surface deformations, i.e. normal vector $\mathbf{N}$ and reflection coefficient ρ.

2.3. **Deflectometry for inner surfaces.** Major purpose of the paper is to adapt the structured lighting-based surface quality control for the inspection of badly accessible inner surfaces.

The major requirements are that (i) the complete inner surfaces to be inspected are illuminated by a structured light, and that (ii) each different defective surface type induces different disturbances of the recorded light pattern.

In the next section, the recording of one surface portion with an optimal light structure is addressed. The achieved results can then be extrapolated to the recording of complete inner surfaces for their quality control.

3. Definition of the most optimal light structure

3.1. **Problem Statement.** As stated in the previous section and in [12], light structure disturbances induced by surface defects must have particular and specific characteristics in order to be discriminated with acceptable surfaces and each other.

As stated in the introduction, the major purpose of the paper is to propose a new method for discriminating different defect types in one shot. The automatic discrimination of 2D and 3D will be addressed. It has been demonstrated previously how these two defect types can be distinguished by means of the induced stripe

disturbances, as the former induce "only" a decrease of light intensity, whereas the latter provoke a change of structure geometry.

The open problem consists of defining the most optimal stripe structure for inner surface recording by means of structured lighting. In accordance to the previous investigations, main challenge consist of adapting the light structure so that all 3D defects can be discriminated (with acceptable surfaces, but also with 2D defective ones). Hence, the problem can be "reduced" to the visual enhancement of 3D geometrical defects on inner surfaces. Once, this achieved, further investigations could address further possible generalization tasks concerning different and/or more complex defects types.

For the 3D defects, these can be simulated by a gaussian function, where the amplitude a gives the defect height, whereas the standard deviation σ is related to the defect width. Depending on the value of these two parameters, such a function can simulate slow varying defect, as dents e.g., mostly due to "hits" of the surface with some external tool, but also deep defect, as pores e.g., due to non optimal surface manufacturing processes. Fig. 3 depicts 2 different 3D defect examples that can be visually enhanced by means of the adapted lighting.

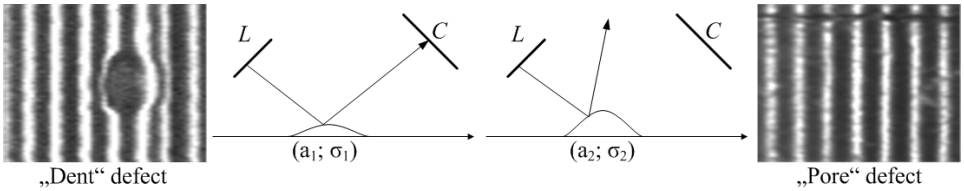

FIGURE 3. Different types of geometrical distortions: (i) Deviation of light structures, "dent-like" defect. The reflected light rays **are** projected onto the sensor. (ii) Decrease of light structures, "pore-like" defect. The reflected light rays **are not** projected onto the sensor.

The figure shows how different 3D defects induce different pattern disturbances. These are, in case of 3D "pore-like" defects, similar to 2D defects. Hence, in case of the considered non-acceptable surfaces, the illumination is optimal for the discrimination of 3D "dent-like" with 3D "pore-like" defects. This is the reason why, only former type of 3D defects will be considered, as the latter is totally described by 2D defect types. Generalization to all possible surface defect types is then straightforward.

Concerning the defect simulation, gaussian functions, as depicted in the Fig. 3, will be used for characterization of dent-like (bump,...) defects. Next section is dedicated to the simulation of distorted light pattern structures.

3.2. **Artificial Image Generation.** In order to facilitate the comparison between different light structures, we simulate the sensor images of a reflected light pattern on the inner surface of a cylindrical workpiece. Hence, for each sensor point ${}^1\mathbf{p}$, corresponding screen point ${}^2\mathbf{p}$ can be computed. Fig. 4 shows the computation principle of the corresponding screen point ${}^2\mathbf{p}$ if the sensor point ${}^1\mathbf{p}$ is known (all the parameters are explained in the text bellow).

It is assumed that the camera center $\mathbf{o} = (0, 0, 0)^{\mathrm{T}}$ is located at the origin of the considered coordinate systems, a cartesian $[\mathbf{x}, \mathbf{y}, \mathbf{z}]$ and a cylindrical $[\mathbf{r}, \varphi, \mathbf{z}]$, with

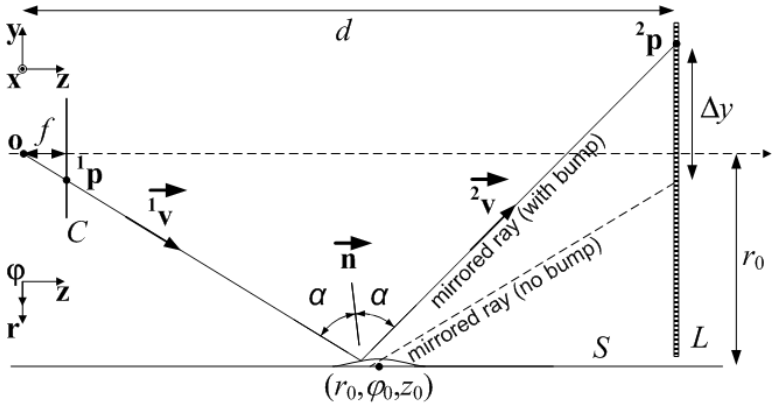

FIGURE 4. Simulation principle based on ray-tracing. The value Δy shows the ray deviation due to the defective surface, which leads to the geometrical light structure deformations.

the camera looking into +**z**-direction. Using a simple perspective pinhole camera model any ray of vision ${}^1\overrightarrow{\mathbf{v}}$ is uniquely defined by its pixel position ${}^1\mathbf{p} = (I_x, I_y)^{\mathrm{T}}$ (from image center) and the focal distance f. Following equation, in the cartesian coordinate system, holds:

$$ {}^1\mathbf{v} = \begin{pmatrix} {}^1v(x) \\ {}^1v(y) \\ {}^1v(z) \end{pmatrix} = \begin{pmatrix} z \cdot I_x/f \\ z \cdot I_y/f \\ z \end{pmatrix} \tag{3.1} $$

The line ${}^1\mathbf{l}$ defined by vector ${}^1\overrightarrow{\mathbf{v}}$ intersects the inner surface S defined by a function f_S. In case of a geometrical distortion, surface's bump is defined by function f_B. The radius of the undistorted (i.e. bumpless) tube is noted r_0, whereas bump's shape and is parametrized by a and σ. For both functions, following equations, in the cylindrical coordinate system, hold:

$$ \mathrm{f}_S^{(\varphi,z)} = (r_0 - \mathrm{f}_B^{(\varphi,z)}; \varphi; z) \tag{3.2} $$

$$ \text{where} \quad \mathrm{f}_B^{(\varphi,z)} = a \cdot \exp\left\{ -\frac{1}{2} \cdot \left(\frac{z - z_0}{\sigma} \right)^2 \right\} \cdot \exp\left\{ -\frac{1}{2} \cdot \left(\frac{\varphi - \varphi_0}{\sigma / r_0} \right)^2 \right\} $$

The bump is centered at position (r_0, φ_0, z_0). In the cartesian coordinate system above equation is defined as:

$$ \begin{aligned} \mathrm{f}_S(x) &= \mathrm{f}_S^{(\varphi,z)} \cdot \cos(\varphi) = \left(r_0 - \mathrm{f}_B^{(\varphi,z)} \right) \cdot \cos(\varphi) \\ \mathrm{f}_S(y) &= \mathrm{f}_S^{(\varphi,z)} \cdot \sin(\varphi) = \left(r_0 - \mathrm{f}_B^{(\varphi,z)} \right) \cdot \sin(\varphi) \\ \mathrm{f}_S(z) &= z \end{aligned} \tag{3.3} $$

With the knowledge of the vector ${}^1\overrightarrow{\mathbf{v}}$ and the surface S, computation of intersection point $\mathbf{M}$ and normal vector $\overrightarrow{\mathbf{n}}$ is straightforward. The Householder matrix permits the computation of the vector ${}^2\mathbf{v}$ of the mirrored line ${}^2\mathbf{l}$:

$$\mathbf{H} = \mathbf{I} - \frac{2}{\mathbf{n}^{\mathrm{T}}\mathbf{n}}\mathbf{n}\mathbf{n}^{\mathrm{T}} \quad \text{where } \mathbf{I} \text{ is the identity matrix} \tag{3.4}$$
$$^{\mathbf{2}}\mathbf{v} = \mathbf{H} \cdot {}^{\mathbf{1}}\mathbf{v}$$

Finally, the parameterized equation of line $^2\mathbf{l}$, defined by vector $^2\overrightarrow{\mathbf{v}}$, allows the computation of the corresponding point $^2\mathbf{p}$ of the structured light screen L.

3.3. **Light Structure Position and Geometry.** The previous investigations [11] showed how far the stripe pattern can be adapted to the surface geometry in order to facilitate quality control. The methodology consisted of recording a regular periodical pattern, in order to facilitate the pattern interpretation. However, in case of the present paper, major constrain is the limited place for positioning and adapting the set-up elements, which are the lighting and the recording sensor.

As stated in section 2.1 one often used method for inner continuous surface inspection (i.e. without bottom) consists of the positioning of the surface to be inspected between the recording sensor and the diffuse lighting.

Thus, the open problem now consists of optimally positioning the structured light pattern to be observed onto the diffusing lighting. Fig. 5 depicts 2 possible light structure positions and 2 possible geometries.

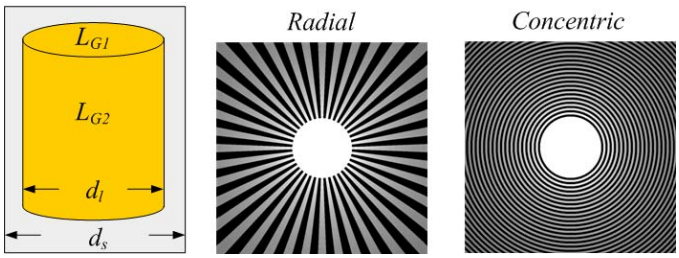

FIGURE 5. Different possible light structure positions and geometries.

Concerning pattern positions, 2 surfaces are possible here: the outer cylindrical L_{G2} and the top circular L_{G1}. The former is the "reverse" solution to the lighting on which this paper is based [11]: the structured light pattern has a cylindrical geometry surrounding the surface to be inspected. However, it has the major disadvantage, that inner surface diameter must be higher than the borescope diameter, i.e. $d_s > d_l$, in order to have enough light rays reflected by the surface and recorded by the camera. Hence, in case of inner surfaces, in order (i) to avoid light intensity problems and (ii) to tackle small inner diameter inspection, latter solution will be retained, i.e. light patterns situated on the top of the circular surface L_{G1}.

For the light pattern geometry, 2 possible solutions are depicted in Fig. 5: the radial and the concentric patterns. The next section will investigate experimentally which pattern geometry is more appropriate for inner surface visual enhancement.

4. Experimental Results

4.1. **Set-Up Description.** The considered set-ups, i.e. the simulated and the real one, where defined with similar parameters. The object radius was approximately $r_0 = 15\ mm$, the camera to pattern distance $d = 150\ mm$, and a focal length

$f = 15\ mm$. The defective surface (the bump), is situated between the optics and the lightings, and characterized by an height and width, $a = 0.15\ mm, \sigma = 1\ mm$. The radial shaped pattern has 40 black and 40 white sectors, which corresponds to a highest frequency of 1 mm, whereas the concentric pattern has a radial spatial frequency of 1 mm.

Concerning the used hardware, the image sequence was taken by using a Dolphin F-145B camera from Allied Vision Technologies, and a Hopkins borescope from Wolf. The pattern was printed using laser printer with a resolution of 1.200 dpi. The object was illuminated by means of a high power LED[1] at 250 mA. Synchronous movement of borescope and pattern was assured by a robot control unit and two linear manipulators. Fig. 6 shows the recording set-up, and the simulated and real images.

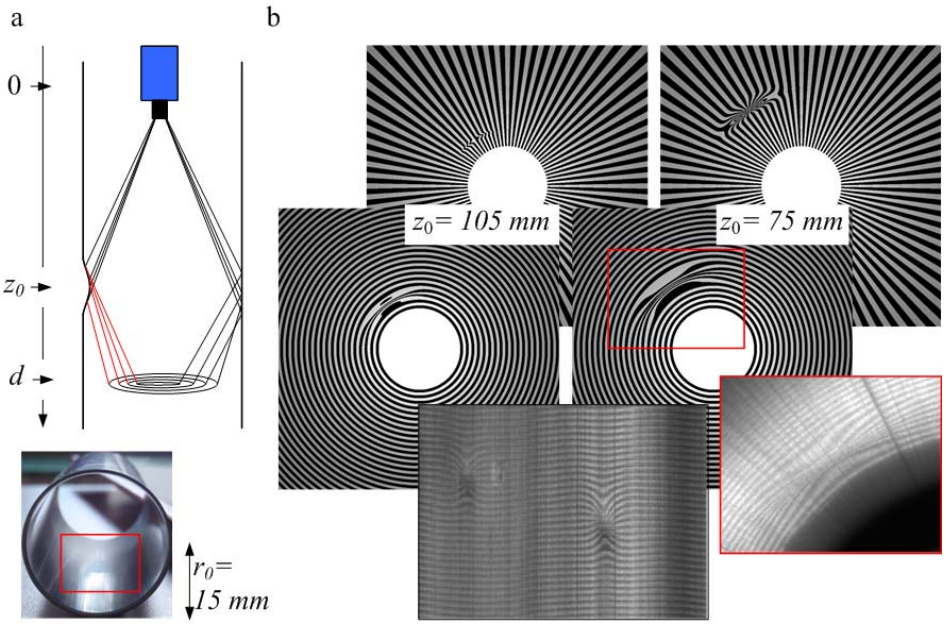

FIGURE 6. Overview of the experimental set-up. Used patterns (radial and concentric). Simulated and recorded images with concentric patterns.

4.2. **Visually Enhanced Surfaces: Simulation.** Following the descriptions of previous section, each structured image can be simulated for each considered light pattern. The images of Fig. 6 show the influence of the defect position on the depicted disturbed light pattern. As state previously 2 pattern geometries, radial and concentric, are considered.

The major disadvantages of the radial pattern are the limits concerning the resolution for pattern generation with a laser printer and pattern recording using a camera. Indeed, most printer have a limited resolution (mostly of 1.200 dpi), so that the central region cannot be displayed properly due to resolution limitations and

[1]Luxeon K2 mit TFFC LXK2-PWC4-0220

moirée effects. Then, the spatial pattern frequency varies with the radius causing higher loss of resolution in the central image regions.

In contrast, the concentric pattern offers a constant pattern frequency, and therefore better printer performance. Moreover, such concentric patterns, once dewarped, offer regular, i.e. with a constant period, light structure. This allows a better and more robust light structure discrimination by means of appropriate data processing approaches, as described in [14].

Nevertheless, resolution limits occurs for all considered light structures, as the spatial structure of the pattern cannot be infinitely small. Indeed, even with a high quality state-of-the-art laser printer at 1.200 dpi (dots per inch), severe moirée effects in the patterns are observed. This effect, occurring when the frequency is higher than approximately 2 mm^{-1}, leads to inadequate image quality.

4.3. **Visually Enhanced Surfaces: Recordings.** Last section showed the major advantages of using a concentric, instead of a radial, pattern. Hence, the recordings of real defects on inner surfaces, have been done by means of a printed concentric pattern, whose period is lower than the width of the defect of approximately 2 mm. Camera resolution was chosen to be at least twice lower than the smallest depicted structure.

The dewarped and fused image depicted in Fig. 6 shows 2 bumps of the tube's shell, which are easily recognizable by the induced disturbances on the light structure. We notice that the recorded images show very similar structures to be characterized, to the stripe structures obtained with the reference application [11]. Hence, same data processing algorithms can be applied in order to automatically discriminate inner defective surfaces. These image content description methods were previously developed and generalized to the characterization of complex bright and dark structures [13, 14].

These recordings show that the proposed method can be applied for real-time inspection systems (same recorded structured images as with the reference system), is very sensitive for the enhancement of geometrical and textural surface perturbations (the resolution is only determined by the printer resolution), and is easy to implement (no special complex hardware is required).

5. Summary and Conclusion

Main purpose of this paper was to propose a new method for inner surface quality control, in order to address complex inspection requirements. Complex means, to be able to discriminate different defect types in one shot. The theoretical developments permit to retrieve the most optimal light structure, so that the final surface recordings show a vertical light pattern, similar to the pattern recorded with the reference inline inspection system.

The reached results prove that it is possible to apply a deflectometry-based technique, to reveal and detect simultaneously different defect types on inner surfaces. The technique is based on the fusion of a diffuse and a structured lighting. To conclude, it has been demonstrated that boreholes with a few millimeter diameter can be inspected so that different defect types can be simultaneously visually enhanced and discriminated. The main parts of these developments were defined for industrial applications successfully integrated in the production lines.

Hence, the applications of the proposed new methodology for the inline inspection are straightforward. These researches will be the basis for the next investigations concerning the inspection of industrial boreholes.

References

1. C. B. Board, *Stress wave analysis of turbine engine faults*, IEEE Aerospace Conference Proceedings, vol. 6, doi:10.1109/AERO.2000.877885, 18-25 March 2000, pp. 79–93.
2. F. Pernkopf., *3D Surface Inspection using Coupled HMMs*, Proc. of the 17th Int. Conf. on Pattern Recognition (ICPR'2004), 2004.
3. F. Pernkopf and P. O'Leary, *Visual inspection of machined metallic high-precision surfaces*, EURASIP Journal on Applied Signal Processing archive **2002** (2002), no. 1, 667–678.
4. Feyzi Inanc, *An optical approach to the characterizations of surface flaws induced by fretting*, AIP Conference Proceedings, vol. 615, doi:10.1063/1.1472877, 2002, pp. 780–787.
5. Jussi Paakkari, *On-Line flatness measurement of large steel plates usinf Moire topography*, Ph.D. thesis, University of Oulu, Finland, 1998.
6. K. Martin, C. V. Stewart, and R. Hammond, *Real time tracking of borescope tip pose*, 3rd IEEE Workshop on Applications of Computer Vision, vol. doi:10.1109/ACV.1996.572016, IEEE Computer Society Press, 02-04 December 1996, pp. 123–128.
7. P. Marino, M.A. Dominguez, and M. Alonso, *Machine-vision based detection for sheet metal industries*, The 25th Annual Conf. of the IEEE Industrial Electronics Society (IECON'1999), vol. 3, 1999, pp. 1330–1335.
8. A. Perelygin and A. A. Chigorko, *Flexible photorecording fiber optical endoscope for the inner wall control of extensive cylindrical article*, Proceedings of the 8th International Scientific and Practical Conference of Students, Post-Graduates and Young Scientists, Tomsk, Russia, vol. doi:10.1109/SPCMTT.2002.1213721, IEEE Operations Center, 8 -12 April 2002.
9. Klaus Spinnler, *Rechteckige Querschnitte kontrollieren*, QZ (Qualität und Zuverlässigkeit) **50** (2005).
10. A. Williams, *Streifenmuster im Spiegelbild*, Inspect Magazine, GIT Verlag GmbH & Co. KG, Darmstadt (2008), no. 02.
11. Yannick Caulier, Andreas Goldschmidt, Klaus Spinnler, and Marc Arnold, *Automatic detection of surface and structural defects on reflecting workpieces*, Photonik Journal **5** (March, 2009).
12. Yannick Caulier, Klaus Spinnler, Salah Bourennane, and Thomas Wittenberg, *New Structured Illumination Technique for the Inspection of High Reflective Surfaces*, EURASIP Journal on Image and Video Processing **2008** (2007), no. 2008, doi:10.1155/2008/237459, 14 pages.
13. Yannick Caulier, Klaus Spinnler, Thomas Wittenberg, and Salah Bourennane, *Segmentation and Classification of Anomalies in Periodic Structures*, Journal of Electronic Imaging **17 (3)** (2008).
14. Yannick Caulier and Salah Bourennane, *Fourier-Based Inspection of Free-Form Reflective Surfaces*, Advanced Concepts for Intelligent Vision Systems (ACIVS 2008), Juan-les-Pins, France, 20-24 October (2008).

Fraunhofer Institute
E-mail address: yannick.caulier@iis.fraunhofer.de